**BIBECHANA**
Vol. 23, No. 3, August 2026, 126–136

ISSN 2091-0762 (Print), 2382-5340 (Online)
Journal homepage: http://nepjol.info/index.php/BIBECHANA
Publisher:Dept. of Phys., Mahendra Morang A. M. Campus (Tribhuvan University)Biratnagar

# Influence of the collecting substrate's nature on structure and properties of *Gajal* soot

**Deepshikha Karki[1,2,3], Bimal Rajchal[1,2,3,4] , Yub Narayan Thapa[1,2,3,5] Motee Lal Sharma[1], Vimal Katiyar[6], Rameshwar Adhikari[1,2,3,6*]**

[1]*Central Department of Chemistry, Tribhuvan University, Kirtipur, Nepal.*
[2]*Research Center for Applied Science and Technology, Tribhuvan University, Kirtipur, Nepal.*
[3]*Nepal Polymer Institute (NPI), Kathmandu, Nepal.*
[4]*Bhaktapur Multiple Campus, Tribhuvan University, Bhaktapur, Nepal.*
[5]*Tribhuvan Multiple Campus, Tribhuvan University, Tansen, Palpa, Nepal.*
[6]*Department of Chemical Engineering, Indian Institute of Technology 781039 Guwahati, Assam, India.*

*Corresponding author: Email: nepalpolymer@yahoo.com

**Abstract**

*Gajal soot, a black carbonaceous residue, was prepared by burning sesame oil with the aid of threaded cotton in a copper oil lamp with the aim of investigating the effect of collecting substrates' nature on the properties of the soot. The substrates made of clay, iron, and bronze were separately used for the collection of the Gajal soot, herein named as GS-CS, GS-IS, and GS-BS, respectively. The physicochemical properties of the soot particles were characterized using UV-visible and Raman spectroscopy, X-ray diffraction (XRD) and Scanning Electron Microscopy (SEM). The disordered structure of each soot particle was revealed by Raman spectra through the appearance of the D-band and G-band around 1336 $cm^{-1}$ and 1590 $cm^{-1}$, respectively. XRD results demonstrated the amorphous nature of soot particles, with crystallite sizes of 1.40 nm, 1.73 nm, and 1.50 nm for GS-CS, GS-IS, and GS-BS, respectively. The agglomerated and irregular-spherical shape of soot particles having a diameter within the range of 20-40 nm for GS-CS and GS-IS, while 40-80 nm for GS-BS, was observed by SEM image. The variation in the particle diameter of soot derived from different substrates was attributed to the collector substrate roughness. The study reveals that the size and optical properties of soot particles show insignificant variation depending on the type of substrate employed for soot collection.*

**Keywords**
Substrate, threaded cotton, oil lamp, disordered structure, nanoparticles.

**Article information**
Manuscript received: May 17, 2026; Revised: August 28, 2026; Accepted: August 29, 2026
DOI: https://doi.org/10.3126/bibechana.v23i3.95942

## 1 Introduction

The incomplete combustion of hydrocarbon fuels generates carbonaceous particles called soot, which is a promising candidate for various scientific applications, including adsorption technology, electronics, catalysis, environmental science, and biomedicine [1, 2]. It is one of the low-cost sources of nanostructured carbon materials, and it consists predominantly of elemental carbon but may also contain varying proportions of inorganic impurities, volatile substances, and organic compounds [3]. Generally, the carbon content, structure, particle size, surface area, and other properties of soot particles depend upon the combustion conditions and precursor fuel [1–5].

Gajal soot is one of the fine and black carbonaceous residues produced through the incomplete combustion of hydrocarbon-based fuels [6], which has been traditionally used as an eye cosmetic [5] and black pigment since the ancient Bronze Age [7, 8]. Different substrates are being used for the collection of Gajal soot. For instance, substrates (in the form of a plate or a bowl) made of clay, copper, bronze, iron or aluminum are used [9, 10]. Similar to other carbonaceous particles, Gajal soot may contain ultrafine carbon nanoparticles with varying degrees of graphitization and surface chemistry [11, 12]. Several studies suggested that several factors, including the substrate, may affect the particle aggregation process, nucleation mechanism, particle growth kinetics, tendency of graphitization, and surface chemistry during soot deposition, thereby influencing the size, crystallinity, and morphology of deposited soot particles [13]. Substrates possessing greater aromatic content are found to contain larger particle aggregates with a higher degree of graphitization, while those with greater oxygen content are found to reduce soot formation [14, 15]. Therefore, scientific evaluation of Gajal soot formation using different substrates and its physicochemical characterization may provide a closer understanding of the effect of substrate on its structural and morphological properties. Analytical techniques such as transmission electron microscopy (TEM), scanning electron microscopy-energy dispersive spectroscopy (SEM-EDS), X-ray diffraction (XRD), Fourier transform infrared (FTIR), and Raman spectroscopy are commonly employed for this purpose.

While most of the existing studies on soot particles are primarily focused on industrial and environmental issues, very little attention has been given to traditional Gajal soot [16–18]. Even though few studies on the structural characterization of Gajal soot have been carried out [6, 19], the systematic investigation on the influence of substrate on the physicochemical features of Gajal soot remains scarce. Since Gajal soot is generally applicable for making Gajal eye cosmetics need to have a small size so that it would not pierce the eyes on application. Therefore, physicochemical characterization of Gajal soot is essential for having deeper insights into its structural composition and morphology. Analytical techniques such as TEM, SEM-EDS, XRD, FTIR, and Raman spectroscopy are commonly employed for this purpose. Several studies depict that soot particles possess an amorphous nature with graphitic layers having particle sizes in the nanometric range, where the particle size varies on the basis of substrates employed for soot collection [9, 19, 20].

The soot particles, which can be prepared by various sources, using different kinds of substrates, and oils, are particularly employed as a precursor for preparing the traditional eye cosmetic Gajal. The art of Gajal making and using it as an eye cosmetic has been followed through generations, adhering to traditional beliefs and culture as a part of Sixteen Sacred Adornment Rituals (Sanskrit: Sodasha Shringaar) [21, 22]. Thus, the study on Gajal soot obtained by varying substrates would deliver a deeper understanding of the structural properties of the soot, thereby better validating their properties from a scientific viewpoint.

The present study aims to assess the effect of substrate on the particle size and optical properties of Gajal soot. It seeks to comparatively evaluate Gajal soot samples generated from the same fuel (sesame oil) but deposited on different substrates (clay, iron, and bronze) using UV-vis, Raman, XRD, and SEM techniques. The findings of this study are expected to contribute toward a better understanding and scientific validation of traditional carbonaceous materials.

## 2 Materials and methods

### 2.1 Materials

Sesame oil, three different kinds of substrates (made up of clay, iron, and bronze), and cotton were purchased from Ashan Tole (local market in Kathmandu), Nepal.

### 2.2 Methods

Five threaded wicks (Nepali: Paanch Sute Batti) of length 9 cm were made from cotton threads by following the traditional Nepalese twisting process for a sacred thread. Then five pieces of five-threaded wicks were dipped in a lamp (Nepali: Diyo) filled with sesame oil (Figure 1(a)). The wicks were ignited and the substrate made of clay was placed 2

cm above the lamp. The smoke released from the flame was deposited on the surface of the clay substrate, leaving behind a black solid residue known as Gajal soot (Figure 1(b)).

Following the same procedure, Gajal soot was also collected on the iron substrate (Figure 1(c)) and bronze substrate (Figure 1(d)) under identical conditions. The resulting soot samples were labelled as Gajal soot derived from clay substrate (GS-CS) (Figure 1(e)), Gajal soot derived from iron substrate (GS-IS) (Figure 1(f)), and Gajal soot derived from bronze substrate (GS-BS) (Figure 1(g)), respectively, for soot collected on clay, iron, and bronze substrates.

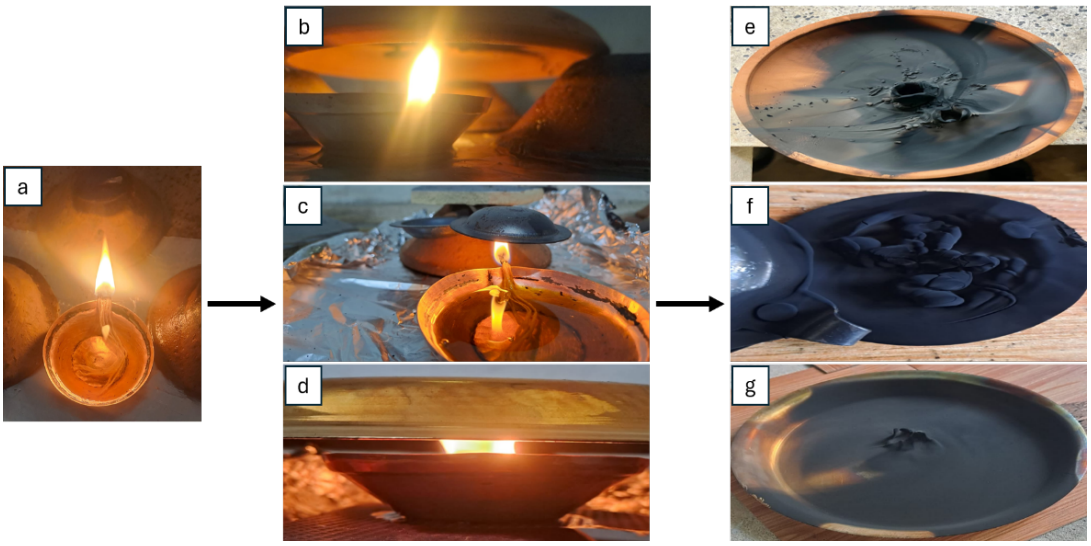


Figure 1: Photograph showing the flame on wick (Nepali: Panch Sute Batti) with aid of sesame oil (a), substrate (clay, iron, and bronze) held over the flame {clay (b), iron (c), and bronze (d)}, and deposition of smoke in form of Gajal soot on substrate {clay (e), iron (f), and bronze (g)}.

## 2.3 Characterization methods

UV-Vis spectroscopy technique was employed to obtain the absorption spectra in the range of 190-600 nm by using a UV 1900 Shimadzu (Japan). Gajal soot of 0.05 mg in 50 mL distilled water was bath sonicated to obtain the dispersion for absorption measurement.

Raman spectra were obtained using a LabRAM HR Evolution RAMAN spectrometer, HORIBA Scientific (Japan), to determine the graphitic phase and disorders in the sample. The excitation wavelength used for Raman measurements was 532 nm. Spectra were obtained in the wavenumber range of 1200 $cm^{-1}$ to 2700 $cm^{-1}$.

X-ray diffraction spectra were obtained using a Rigaku X-ray diffractometer D/teX Ultra 250 (Japan) with Cu-K$\alpha$ radiation of wavelength 1.541 Å. The spectra were recorded from 10° to 90°. The spectra were analyzed using Gauss' function. The crystallite size of the soot was calculated using the Debye-Scherrer equation (1).

$$L_a = \frac{K\lambda}{\beta \cos\theta} \quad (1)$$

where,

$L_a$ = crystallite size, $K$ = Scherrer constant (0.9), $\beta$ = full width at half maximum (FWHM) in radians, and $\lambda$ = wavelength (0.154 nm).

Field Emission Scanning Electron Microscopy (FE-SEM) of Zeiss Gemini 500 (Germany), was employed to study the surface morphology of Gajal soot. A small amount of sample was sprayed on a double-sided carbon tape mounted on aluminum stubs, gold sputtered and loaded on a movable stage of a microscope. The sample's surfaces were scanned at a magnification of 500,000x to obtain the image. The particle size of the samples was calculated using ImageJ software.

# 3 Results and discussion

## 3.1 Clay substrate-derived Gajal soot (GS-CS)

Figure 2 shows the UV-vis and Raman spectra, XRD diffractogram and FESEM micrograph of GS-CS. The UV-vis spectrum of GS-CS in Figure 2(a) displayed an absorption spectrum with two peaks located around 227 nm and 255 nm. The absorption of UV-vis radiation by carbon materials depends on the internal structure and electronic transition be-

tween bonding and anti-bonding orbitals [15]. It is reported that the peak located in the range of 180-270 nm is attributed to $\pi-\pi^*$ transitions associated with the presence of a C=C double bond [23, 24]. Thus, the UV-vis peak in the present study, located around 260 nm, can be attributed to a $\pi-\pi^*$ transition arising from the C=C double bond, indicating the presence of graphitic carbon in the soot particles containing $sp^2$ hybridized carbon atoms.

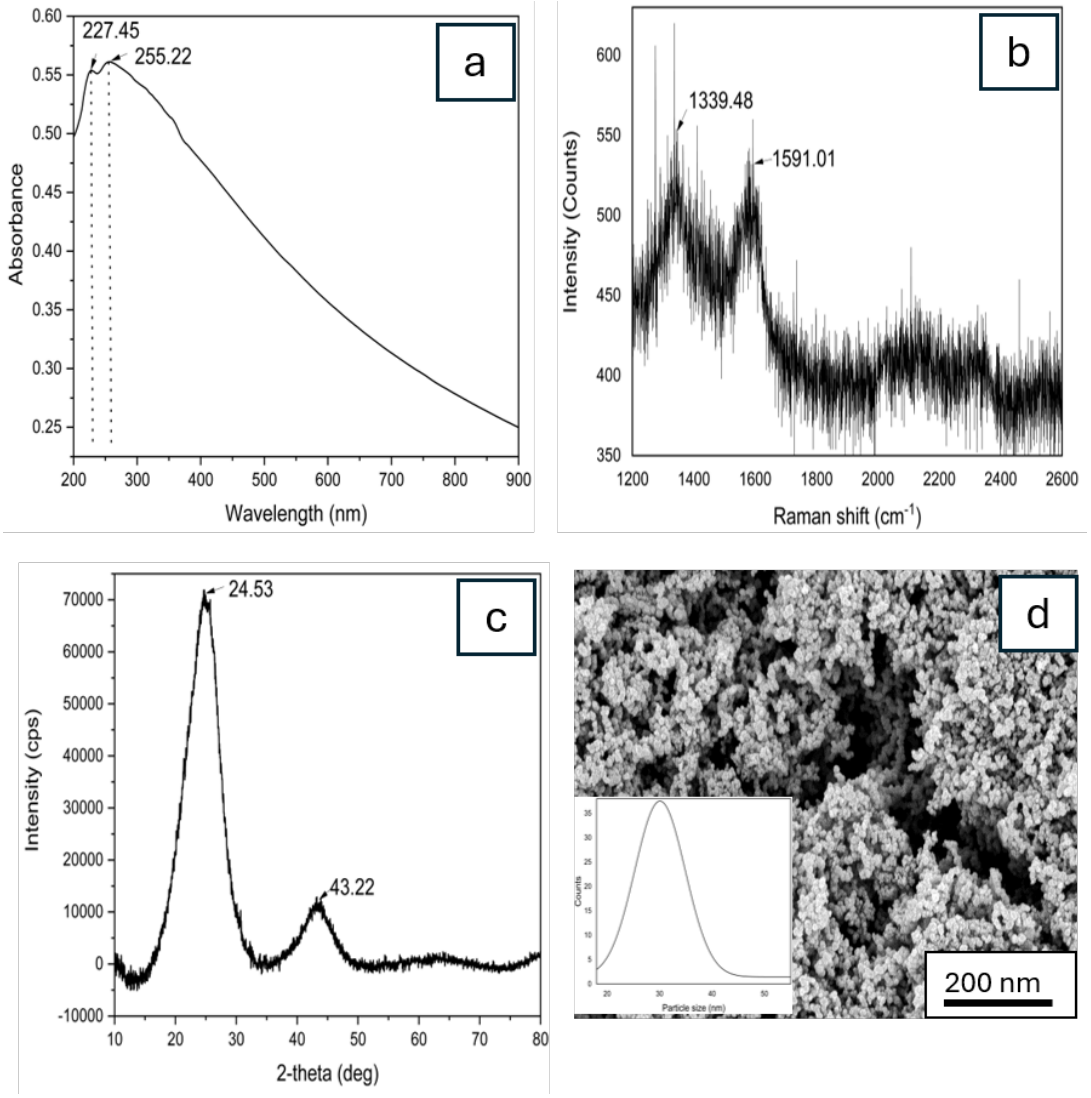


Figure 2: Structural and morphological analysis using UV-vis spectra (a), Raman spectra (b), XRD pattern (c), and FESEM micrograph along with histogram at the lower left corner indicating the range of particle size (d) of GS-CS.

Raman spectra provide information on the presence of defects and on the ordered or disordered structure of soot particles. The Raman spectrum presented in Figure 2(b) depicted two peaks positioned at wavenumbers 1339.48 $cm^{-1}$ and 1591.01 $cm^{-1}$. It is known that the peak at 1343 $cm^{-1}$ corresponds to the D-band, indicating the presence of $sp^3$ hybridized carbon along with the presence of defects or amorphous structure in the soot particles, while the peak at 1591 $cm^{-1}$ corresponds to the G-band, which indicates the presence of $sp^2$ hybridized carbon with graphitic structure [25–27]. The proximity of observed peaks to earlier studies thus supports the presence of $sp^2$ and $sp^3$ hybridized carbon, as indicated in UV-vis results, and indicates the presence of a disordered structure of GS-CS.

The X-ray diffractogram of GS-CS in Figure 2(c) depicts peaks reflected at $2\theta$ values of 24.53° and 43.22°, followed by a broad hump. The peak intensity at 24.53° can be attributed to (002) indices indicating a graphitic carbon layer, while the peak at 43.21° is attributed to (100) indices because of in-plane hexagonal graphitic lattice reflection [1, 28].

The appearance of a noticeable broad hump is an indication of the presence of an oxygen-containing group on the surface of soot particles [29]. The average crystallite size of soot particles was found to be 1.40 nm (Table 1). The calculated crystallite size indicated a lower degree of order and graphitization for GS-CS [30]. The XRD peak position in GS-CS is consistent with the reported study [24, 31].

FESEM micrograph of GS-CS in Figure 2(d) displays the presence of agglomerated particles in the sample with particle diameters within the range of 20 to 40 nm. The particle size of GS-CS determined through the FESEM micrograph is consistent with the size of soot particles reported in the earlier study [12].

In summary, GS-CS contains $sp^2$ and $sp^3$ hybridized carbon structures with C-C/C=C bonds as displayed by UV-vis and Raman spectra. The disordered structure suggested by the Raman spectrum holds good on the XRD pattern, from which an average crystallite size was calculated and was found to be 1.40 nm, that indicate the presence of amorphous (partially ordered) carbon in soot particles. The particle diameter measured from the FESEM image is from 20 to 40 nm.

Table 1: Crystallite size calculation of GS-CS by using the Debye-Scherrer equation

| k | $\lambda$ | $2\theta$ | FWHM | $\beta$ (RAD) | Crystallite size | Average D (nm) |
|---|---|---|---|---|---|---|
| 0.94 | 0.154 | 24.53 | 6.68 | 0.12 | 1.27 | 1.40 |
| 0.94 | 0.154 | 43.23 | 5.81 | 0.10 | 1.53 | |

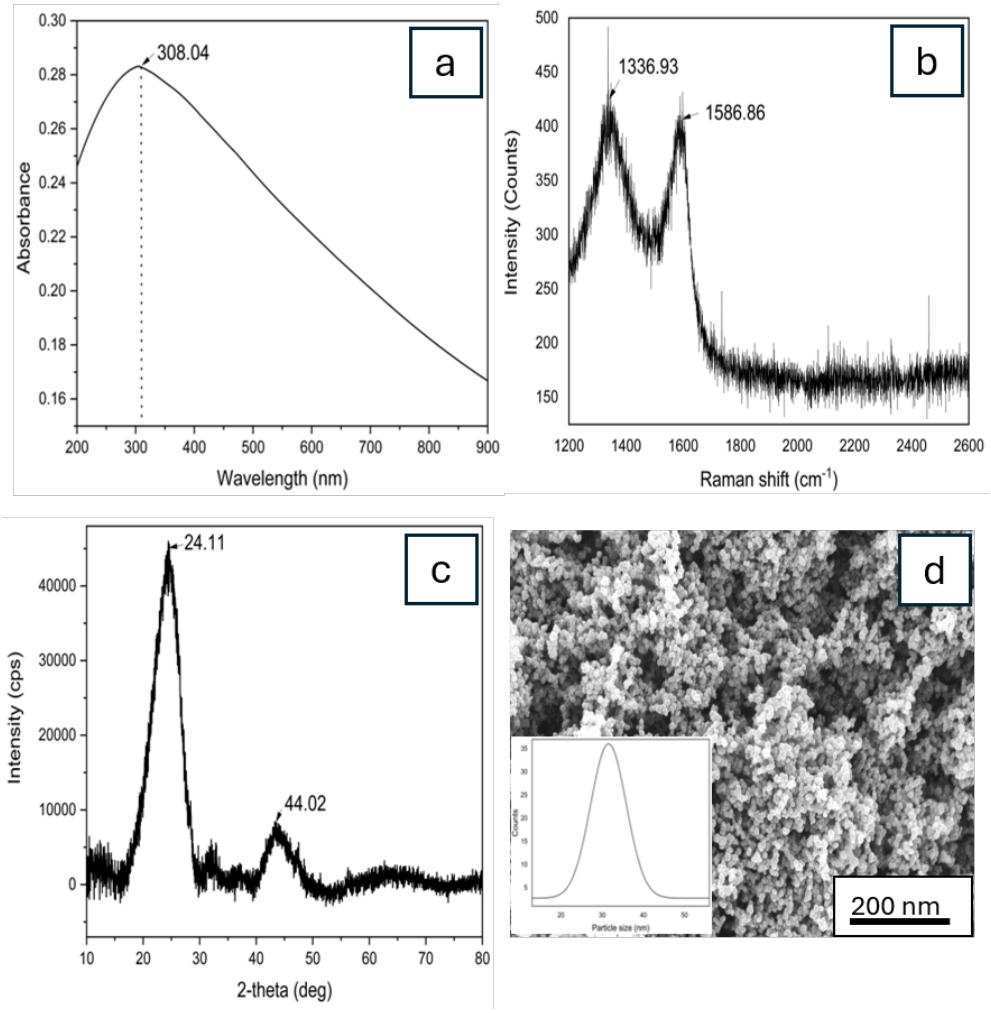


Figure 3: Structural and morphological analysis using UV-vis spectra (a), Raman spectra (b), XRD pattern (c), and FESEM micrograph along with histogram at the lower left corner indicating the range of particle size (d) of GS-IS.

### 3.2 Iron substrate-derived soot (GS-IS)

Figure 3 shows UV-vis and Raman spectra, XRD diffractogram, and FESEM micrograph of GS-IS. Similar to the soot obtained onto a clay substrate, the sample prepared on the iron substrate showed the absorption peak that was attributed to $\pi - \pi^*$ transition corresponding to the C-C, C=C, and C=O bonds [32, 33] but revealed a single peak located around 308 nm (Figure 3(a)), double Raman peaks located at 1336.93 $cm^{-1}$ and 1586.86 $cm^{-1}$ (Figure 3(b)) [18, 34]. XRD peaks centered at $2\theta$ values of 24.11° and 44.02° (Figure 3(c)) [16, 28, 35, 36]. This observation implies that GS-IS has similar structural and optical property as to the properties to those obtained from GS-CS. The average crystallite size of GS-IS soot particles was found to be 1.73 nm (Table 2). The FESEM image (Figure 3(d)) of GS-IS is identical to that of GS-CS.

However, the UV-vis absorption peak was located around 308 nm, which may arise due to oxidation of graphene basal planes or the presence of micro- to nano-sized particles [14, 17, 24, 37]. The slight shifting of Raman peak position from 1339.48 $cm^{-1}$ to 1336.93 $cm^{-1}$ and 1591.01 $cm^{-1}$ to 1586.86 $cm^{-1}$, compared to GS-CS, indicated that both disordered and graphitic structures were simultaneously decreased by a few magnitudes in GS-IS.

Such a shifting of the peak position may be due to the conversion of $sp^3$ bonds to $sp^2$ bonds in soot particles because of the metal substrate, which attained rapid heating during soot deposition, whereas the clay substrate required a comparatively longer time to attain a similar temperature, despite the flame height and number of wicks being maintained constant throughout the experiment [38].

The $2\theta$ value indicating the amorphous nature of [39] GS-CS and particle diameter is consistent with the literature [11, 16, 28, 35, 36].

Table 2: Crystallite size calculation of GS-IS by using the Debye-Scherrer equation

| k | $\lambda$ | $2\theta$ | FWHM | $\beta$ (RAD) | Crystallite size | Average D (nm) |
|---|---|---|---|---|---|---|
| 0.94 | 0.154 | 24.41 | 5.72 | 0.09 | 1.48 | 1.73 |
| 0.94 | 0.154 | 44.02 | 4.49 | 0.078 | 1.99 | |

Table 3: Crystallite size calculation of GS-BS by using the Debye-Scherrer equation

| k | $\lambda$ | $2\theta$ | FWHM | $\beta$ (RAD) | Crystallite size | Average D (nm) |
|---|---|---|---|---|---|---|
| 0.94 | 0.154 | 24.57 | 6.35 | 0.11 | 1.33 | 1.50 |
| 0.94 | 0.154 | 43.37 | 5.32 | 0.09 | 1.67 | |

### 3.3 Bronze substrate-derived Gajal soot (GS-BS)

Figure 4 shows the structure of GS-BS, employing UV-vis spectrum (Figure 4(a)), Raman spectrum (Figure 4(b)), and XRD pattern (Figure 4(c)) is identical to those of GS-IS. The disordered structure supporting the presence of $sp^2$ and $sp^3$ hybridized carbon is consistent with the literature [14, 40–42]. The crystallite size was found to be 1.50 nm (Table 3). The morphology of GS-BS from FESEM aligned with that of GS-IS, but the calculated particle diameter range of GS-BS is more than that of GS-IS and is found to be 40-80 nm (Figure 4(d)). The structure and morphology of the soot particles are consistent with earlier reported studies [1, 19, 43, 44].

### 3.4 Overall discussion and summary

The UV-Vis spectroscopy of the Gajal soot displayed an absorption peak in the range of 227 nm to 308 nm, indicating that the electronic transition was due to C-C, C=C, or C=O double bonds and the presence of carbon nanoparticles in soot particles. Furthermore, GS-CS showed two absorption peaks while GS-IS and GS-BS disclosed only one absorption peak. Raman spectra of the detected soot particles revealed the disordered structure of Gajal soot through the appearance of the D-band and G-band, which supports the UV-vis spectra.

Furthermore, the XRD diffractogram of GS-CS and GS-IS disclosed one peak reflected around a $2\theta$ value of 24° and another peak around 43.3°, followed by a noticeable hump around 62°, while GS-BS shows only two peaks at 24.57° and 43.37°. The reflected peaks in XRD in the range of 22°-24° and

42°-45° were attributed to the amorphous nature of carbon, as the peak appeared to be broad [44]. The present study also revealed the amorphous nature of soot particles, which was further supported by their crystallite sizes. The crystallite sizes of GS-CS, GS-IS, and GS-BS were found to be 1.40 nm, 1.73 nm, and 1.50 nm, respectively, which clarified that the soot particles possessed partially ordered carbon (lower degree of order and graphitization as supported by Raman spectra), indicating the predominantly amorphous nature of soot particles. The overall particle size of prepared GS-CS and GS-IS was found in the range of 20-40 nm, while that of GS-BS was in the range of 40-80 nm, confirming the nanoparticulate morphology of the soot particles.

Although the soot particles derived using three different substrates exhibited a partially ordered nature, characteristic distinctions between those particles were observed during spectroscopic and microscopic analysis. There is only a slight variation in the position of the absorption peak and Raman wavenumbers. Similarly, minimal variation in crystallite size and particle size of soot has been investigated. These differences in particle size and optical properties are attributed to the substrate's surface, employed for soot collection, where soot particles get adsorbed. The surface of clay substrates was highly rough and porous, while the bronze substrate's surface was smooth and plain, and the surface of the iron substrate was intermediate between clay and bronze [45]. The binding of soot molecules directly to the surface of the substrate may be due to physical adsorption, depending on the roughness of the substrates. The earlier study reported the inverse relationship between adsorption of soot particles to the rough/smooth substrate [46].

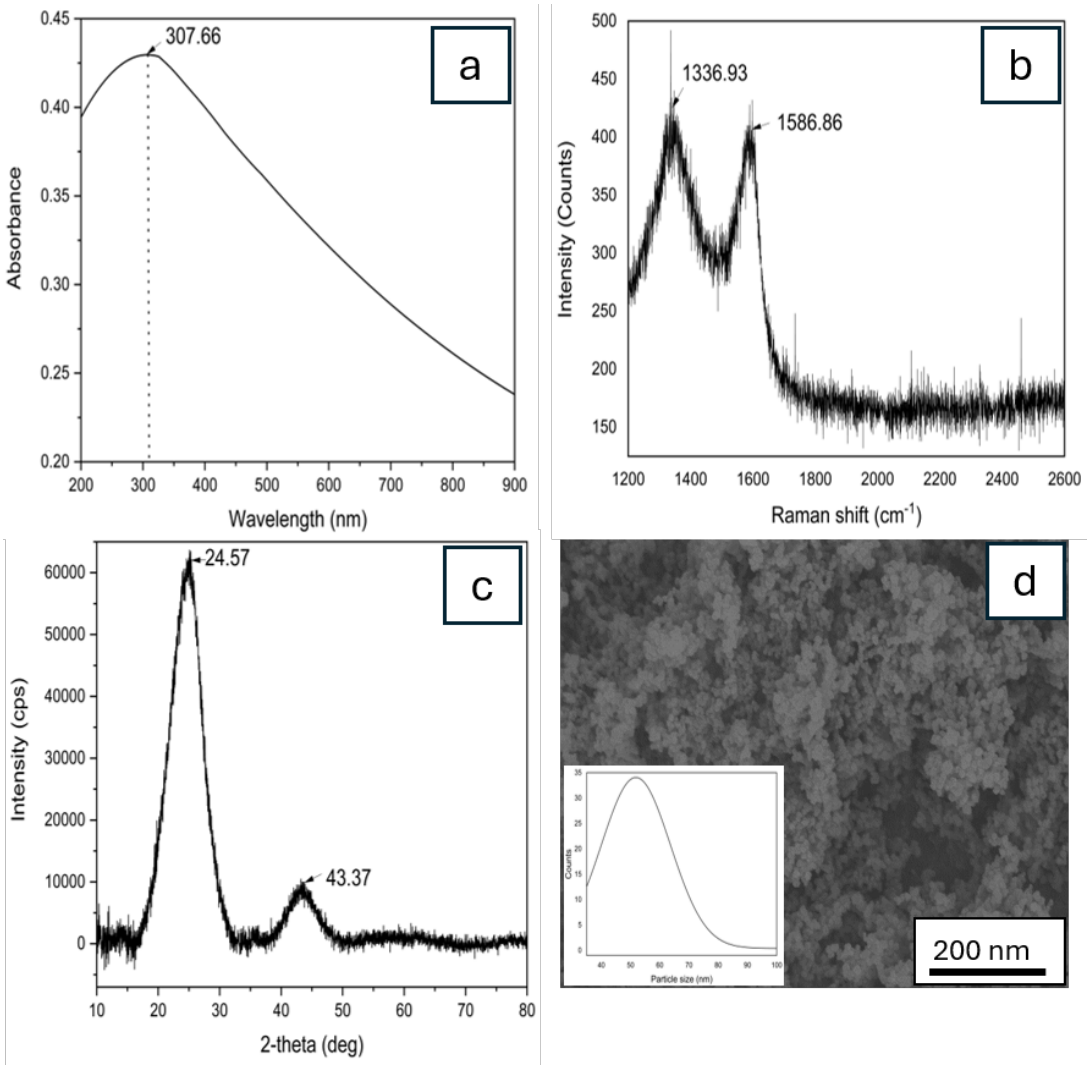


Figure 4: Structural and morphological analysis using UV-vis spectra (a), Raman spectra (b), XRD pattern (c), and FESEM micrograph along with histogram at the lower left corner indicating the range of particle size (d) of GS-BS.

Although the soot particles derived using three different substrates exhibited a partially ordered nature, characteristic distinctions between those particles were observed during spectroscopic and microscopic analysis. There is only a slight variation in the position of the absorption peak and Raman wavenumbers. Similarly, minimal variation in crystallite size and particle size of soot has been investigated. These differences in particle size and optical properties are attributed to the substrate's surface, employed for soot collection, where soot particles get adsorbed. The surface of clay substrates was highly rough and porous, while the bronze substrate's surface was smooth and plain, and the surface of the iron substrate was intermediate between clay and bronze [45]. The binding of soot molecules directly to the surface of the substrate may be due to physical adsorption, depending on the roughness of the substrates. The earlier study reported the inverse relationship between adsorption of soot particles to the rough/smooth substrate [46].

Additionally, despite keeping the number of wicks and amount of oil constant, the heating behavior of the clay, iron, and bronze substrates may vary. Since metals get heated and cooled faster than the clay substrate, the extent of conversion of $sp^3$ to $sp^2$ hybridized carbon may take place more immediately in the metal substrate than in the clay substrate [38]. The clay substrate may take some more time to be heated and cooled in comparison to the metal substrate; the structure of metal-derived soot particles was found to have a comparatively ordered structure than the clay substrate-derived soot particles.

Table 4: Comparative analysis of Gajal soot derived from different substrates using sesame oil.

| **S. N.** | **Substrate** | **UV-vis** (nm) | **Raman** ($cm^{-1}$) | **XRD** | **FESEM** (nm) | **Remarks** |
|---|---|---|---|---|---|---|
| 1. | Clay | 227.45, 255.22 | 1339.48, 1591.01 | 24.53°, 43.21° | 20-40 | Present study |
| 2. | Iron | 308.04 | 1336.93, 1586.86 | 24.11°, 44.02° | 20-40 | Present study |
| 3. | Bronze | 307.66 | 1336.93, 1586.86 | 24.57°, 43.37° | 40-80 | Present study |
| 4. | Steel | - | 1350.00, 1595.00 | 25.40°, 43.80° | 50-70 | Ref. [47] |
| 5. | Glass | - | - | 20-22° | 60-70 | Ref. [48] |

Further, it has been reported that the soot particles are externally oxidized by carbon dioxide ($CO_2$), water ($H_2O$) molecules, and hydroxyl (-OH) to maintain the particle size [49]. During the process, it may be expected that these $CO_2$, $H_2O$, and -OH groups, which influence the particle size, agglomeration and surface growth of soot particles [50], may also play a role in the interaction of soot particles with porous/rough substrates more readily than on smooth substrates. Here, iron and bronze are both metals, but the surface of the iron substrate was rougher than that of bronze. As a result, the soot particles derived from substrates with rough surfaces have particle sizes in the range of 20-40 nm (GS-CS and GS-IS), while those from smooth surfaces (GS-BS) possess soot particle sizes in the range of 40-80 nm.

The comparative assessment of substrates' effect on particle size and optical properties of Gajal soot particles derived from different substrates is further supported by earlier studies, which disclose that soot particles derived from steel and glass substrates possess smooth surfaces and have a particle size in the range of 50-70 nm [47, 48]. The comparison of the particle size and optical properties of Gajal soot obtained by varying the substrate is indexed in Table 4.

The observed insignificant variation in particle size may be attributed to the substrate, considering that soot formation occurs through a series of sequential processes within the flame that comprise precursor formation, nanoparticle formation, primary soot formation, and aggregate formation [51], where the particle size is already maintained. Since the precursor (sesame oil), wick, distance between lamp and substrate, and time taken for complete extinction of flame were constant during soot collection, the overall particle size range varies insignificantly.

The study suggests that the degree of agglomeration or the size of particles changes within the flame; however, there might be less chance where the substrate surface does take part in such changes [52].

## 4 Conclusion

This study provides detailed information about the substrate's effect on particle size and structural properties of Gajal soot prepared by varying the substrates. The soot particles possess a very low degree of order and graphitization, indicating the amorphous nature of carbon. Additionally, the minimal variation in the particle size of soot resulted from the smoothness and roughness of the substrate. Hence, substrate variation ultimately leads to insignificant changes in the particle size and structure of Gajal soot.

The UV-vis and Raman spectra and XRD diffractogram have revealed the partially ordered structure of Gajal soot derived from all the substrates (clay, iron, and bronze), while the FESEM imaging indicates the minimal role of surface roughness in the soot particle size variation. Thus, the substrate variation leads to insignificant changes in their particle size and optical properties. Since the Gajal soot is generally prepared from a cosmetic point of view, its potential activity against bacterial infections needs to be further explored to ensure its safety and efficacy.

### Funding statement

This research received no external funding.

### Conflict of Interest

There is no conflict to declare. All authors have read, made necessary corrections, and approved the final version of the manuscript.

### Acknowledgements

The authors would like to acknowledge the 'Centre for International Migration and Development (CIM)' for the donation of a UV-vis spectrophotometer, brought under the returnee's fellowship of Mr. Ramesh Puri, and for his collaborative support and fruitful discussions. The authors also acknowledge the University Grants Commission (UGC) for supporting the RECAST laboratory through different projects.

### Authors' contributions

**DK:** Investigations, Manuscript Draft Preparation, Data Analysis, and Interpretation
**BR:** Manuscript Draft Preparation, Data Analysis, and Interpretation
**YNT:** Manuscript Draft Preparation, Data Analysis, and Interpretation
**MLS:** Editing, Reviewing, Supervision
**VK:** Editing, Reviewing, Supervision, Resources
**RA:** Conceptualization, Editing, Reviewing, Supervision

### References

[1] Singh S, et al. Candle Soot-Derived Carbon Nanoparticles: An Inexpensive and Efficient Electrode for Microbial Fuel Cells. Electrochimica Acta. 2018;264:119-27.

[2] Liu Y, et al. Evaluation of the Oxidative Reactivity and Electrical Properties of Soot Particles. Carbon. 2021;178:37-47.

[3] Michelsen HA, et al. A Review of Terminology Used to Describe Soot Formation and Evolution under Combustion and Pyrolytic Conditions. ACS Nano. 2020;14:12470-90.

[4] Jayaprakasan MV, et al. Nanocarbon Material from Edible Oils: Synthesis and Characterization. IOSR Journal of Applied Physics. 2013;3:51-8.

[5] Adhikari R. Traditional Nanotechnology of Nepal. Nanomaterials and Polymer Innovation. 2025;1:58-60.

[6] Jayaprakasan MV. Nanocarbon Material from Edible Oils: Synthesis and Characterization. IOSR Journal of Applied Physics. 2013;3:51-8.

[7] Ben-Nun L. Medical Effects of Cosmetics. Beer-Sheva, Israel: B.N. Publication House; 2016. Available from: https://www.researchgate.net/publication/296485304.

[8] Sharma RK, et al. Anjanam (Eye Care in Ayurveda). International Journal of Research in Medical Sciences and Technology. 2019;8.

[9] Baskar R. Analysis of Nano Carbon Obtained from Mustard Oil Soot. Indian Institute of Technology (Chennai); 2017.

[10] Tamang S, et al. Green Synthesis, Characterization, and Antimicrobial Activity of Carbon Nanoparticles Derived From Mustard Oil. Amrit Research Journal. 2025;5:91-7.

[11] S S. Synthesis and Characterization of Carbon Nano Kajal. Juniper Online Journal of Material Science. 2017;1.

[12] Randive DS, et al. Carbon-Based Kajal Formulations: Antimicrobial Activity and Feasibility as a Semisolid Base for Ophthalmics. Journal of Pharmaceutical Research International. 2020;32:62-74.

[13] Martin JW, et al. Soot Inception: Carbonaceous Nanoparticle Formation in Flames: Soot Inception. Progress in Energy and Combustion Science. 2022;88:100956.

[14] Russo C, et al. Spectral Analysis in the UV-Visible Range for Revealing the Molecular Form of Combustion-Generated Carbonaceous Species. Combustion Science and Technology. 2012;184:1219-31.

[15] Jäger C, et al. Spectral Properties of Carbon Black. Journal of Non-Crystalline Solids. 1999;258:161-79.

[16] Dikio ED. Morphological Characterization of Soot from the Atmospheric Combustion of Kerosene. Journal of Chemistry. 2011;8:1068-73.

[17] Swapna MS, Sankararaman S. Blue Light Emitting Diesel Soot for Photonic Applications. Materials Research Express. 2018;5.

[18] Shooto ND, Dikio ED. Synthesis and Characterization of Diesel, Kerosene and Candle Wax Soot's. International Journal of Electrochemical Science. 2012;7:4335-44.

[19] Pahal V, et al. Characterization and Comparative Assessment of Bactericidal Activity of Carbon Nanodots (CDs) and Nanoparticles (CNPs) Prepared from Soot's of Clarified Butter and Mustard Oil, Respectively. Journal of Applied Biology & Biotechnology. 2023;11:233-48.

[20] Muhsan MS, et al. Synthesis of Carbon Nanoparticles by Using Seed Oils. Pakistan Journal of Scientific & Industrial Research Series A: Physical Sciences. 2019;62:1-7.

[21] Husain N, Khalid M. Aesthetic Significance of Solah Shringar (Sixteen Ornaments) in Unani Medicine. Journal of Complementary and Alternative Medical Research. 2021;15:69-81.

[22] Ghimire HL. A Study of Living Godess Kumārī: The Source of Cultural Tourism in Nepal. Gaze: Journal of Tourism and Hospitality. 2018;9:23-42.

[23] Sharif Sh M, et al. Dispersion and Stability of Carbon Black Nanoparticles, Studied by Ultraviolet–Visible Spectroscopy. Journal of the Taiwan Institute of Chemical Engineers. 2009;40:524-7.

[24] Andrijanto E, et al. Facile Synthesis of Graphene from Graphite Using Ascorbic Acid as Reducing Agent. In: AIP Conference Proceedings; 2016. p. 020003.

[25] Knight DS, White WB. Characterization of Diamond Films by Raman Spectroscopy. Journal of Materials Research. 1989;4:385-93.

[26] Ahmed S, et al. Investigation on Activated Carbon Derived from Biomass Butnea Monosperma and Its Application as a High Performance Supercapacitor Electrode. Journal of Energy Storage. 2019;26:100988.

[27] Lamsal B, et al. Facile Synthesis of Disordered Graphitic Charcoal by Direct Pyrolysis of Mustard Oil Cake and Sugarcane Bagasse. Advanced Materials Letters. 2025:1-8.

[28] Mohan AN, Manoj B. Synthesis and Characterization of Carbon Nanospheres from Hydrocarbon Soot. International Journal of Electrochemical Science. 2012;7:9537-49.

[29] Venkatesan S, et al. Fuel Waste to Fluorescent Carbon Dots and Its Multifarious Applications. Sensors and Actuators B: Chemical. 2019;282:972-83.

[30] Sadezky A, et al. Raman Microspectroscopy of Soot and Related Carbonaceous Materials: Spectral Analysis and Structural Information. Carbon. 2005;43:1731-42.

[31] Zhang W, et al. Preparation of Carbon Nanoparticles from Candle Soot. Chemistry Letters. 2009;38:28-9.

[32] Anu NM, Manoj B. Exploration of Carbon Nano Dots in Hydro Carbon Soot and Carbon Black. Research Journal of Chemistry and Environment. 2017;21:1-6.

[33] Chandra S, et al. Mustard Seeds Derived Fluorescent Carbon Quantum Dots and Their Peroxidase-like Activity for Colorimetric Detection of $H_2O_2$ and Ascorbic Acid in a Real Sample. Analytica Chimica Acta. 2019;1054:145-56.

[34] Cuesta A, et al. Raman Microprobe Studies on Carbon Materials. Carbon. 1994;32:1523-32.

[35] Olifant GE, et al. Application of Candle Soot CNPs-$TiO_2$-PVP Composite in the Detection of Volatile Organic Compounds with Aldehyde, Amine and Ketone Functional Groups by Resistance and Impedance Responses. Nano Express. 2021;2:020010.

[36] Hossain MA, Islam S. Synthesis of Carbon Nanoparticles from Kerosene and Their Characterization by SEM/EDX, XRD and FTIR.

American Journal of Nanoscience and Nanotechnology. 2013;1:52-6.

[37] Sahoo BN, Kandasubramanian B. Photoluminescent Carbon Soot Particles Derived from Controlled Combustion of Camphor for Superhydrophobic Applications. RSC Advances. 2014;4:11331.

[38] Swapna MS, et al. Camphor Soot: A Tunable Light Emitter. Applied Physics A. 2018;124:50.

[39] Takagi H, et al. XRD Analysis of Carbon Stacking Structure in Coal during Heat Treatment. Fuel. 2004;83:2427-33.

[40] Matthews MJ, et al. Origin of Dispersive Effects of the Raman D Band in Carbon Materials. Physical Review B. 1999;59:R6585-8.

[41] Joshi P, et al. Characterization of Carbon Derived from Candle by Flame-Soot Method for Counter Electrodes of Dye-Sensitized Solar Cells. BIBECHANA. 2023;20:205-12.

[42] Sharma V, et al. Graphene Synthesis via Exfoliation of Graphite by Ultrasonication. International Journal of Engineering Trends and Technology. 2015;26:37-42.

[43] Han SW, et al. Effect of Pyrolysis Temperature on Carbon Obtained from Green Tea Biomass for Superior Lithium Ion Battery Anodes. Chemical Engineering Journal. 2014;254:597-604.

[44] Taer E, et al. The Synthesis of Activated Carbon Made from Banana Stem Fibers as the Supercapacitor Electrodes. Materials Today: Proceedings. 2021;44:3346-9.

[45] Hussein HA, et al. Superhydrophobic Candle Soot Coating Directly Deposited on Aluminum Substrate with Enhanced Robustness. Coatings. 2022;12(2):202.

[46] Tan CLC, et al. Adhesion of Dust Particles to Common Indoor Surfaces in an Air-Conditioned Environment. Aerosol Science and Technology. 2014;48:541-51.

[47] Tyagi A, et al. Optimization of *Sesamum Indicum* Oil (Sesame Oil) Derived Activated Carbon Soot for Electric Double-Layer Capacitor (EDLC) Application. Biomass Conversion and Biorefinery. 2024;14:19349-67.

[48] Jayaprakasan MV, et al. Synthesis of Nanocarbon Powder from Sesame Oil and Its SEM Characterization. International Journal of Scientific and Research Publications. 2013;3.

[49] Faeth G, et al. Soot Surface Growth and Oxidation in Diffusion Flames at Subatmospheric and Atmospheric Pressures. In: 41st Aerospace Sciences Meeting and Exhibit. Reston, Virginia: American Institute of Aeronautics and Astronautics; 2003. p. 43-57.

[50] D'Anna A. Kinetics of Soot Formation. Elsevier Inc.; 2015. .

[51] Martin JW, et al. Soot Inception: Carbonaceous Nanoparticle Formation in Flames. Progress in Energy and Combustion Science. 2022;88:100956.

[52] Dobbins RA, Megaridis CM. Morphology of Flame-Generated Soot as Determined by Thermophoretic Sampling. Langmuir. 1987;3:254-9.